Universiteit Antwerpen

This item is the archived peer-reviewed author-version of:

Demonstration of a 2 × 2 programmable phase plate for electrons

Reference:
Verbeeck Johan, Béché Armand, Müller-Caspary Knut, Guzzinati Giulio, Luong Mihn Anh, Den Hertog Martien.- Demonstration of a 2 × 2 programmable phase plate for electrons
Ultramicroscopy - ISSN 0304-3991 - 190(2018), p. 58-65
Full text (Publisher's DOI): https://doi.org/10.1016/J.ULTRAMIC.2018.03.017
To cite this reference: https://hdl.handle.net/10067/1504590151162165141

uantwerpen.be
Institutional repository IRUA

Demonstration of a 2x2 programmable phase plate for electrons

Jo Verbeeck [a] Armand Béché [a] Knut Müller-Caspary [a]
Giulio Guzzinati [a] Minh Anh Luong [b] Martien Den Hertog [c]

[a] *EMAT, University of Antwerp, Groenenborgerlaan 171, 2020 Antwerp, Belgium.*

[b] *Univ. Grenoble Alpes, CEA, INAC, MEM, LEMMA Group, F-38000 Grenoble, France*

[c] *Institut Neel, 25 avenue des Martyrs BP 166, 38042 Grenoble Cedex 9, France.*

Abstract

First results on the experimental realisation of a 2x2 programmable phase plate for electrons are presented. The design consists of an array of electrostatic elements that influence the phase of electron waves passing through 4 separately controllable aperture holes. This functionality is demonstrated in a conventional transmission electron microscope operating at 300 kV and results are in very close agreement with theoretical predictions. The dynamic creation of a set of electron probes with different phase symmetry is demonstrated, thereby bringing adaptive optics in TEM one step closer to reality. The limitations of the current design and how to overcome these in the future are discussed. Simulations show how further evolved versions of the current proof of concept might open new and exciting application prospects for beam shaping and aberration correction.

Key words: electron optics, phase plate, beam forming, electrostatic lens, adaptive optics

1 Introduction

Adaptive optics, the technology to dynamically change the phase transfer of optical elements has its roots in astrophysics, where dynamically changing telescope mirrors can compensate for time varying atmospheric induced aberrations for optimised observation from earth [1–4], as well as in space [5].

Email address: jo.verbeeck@uantwerp.be (Jo Verbeeck).

The technology has greatly improved since and has sparked an avalanche of innovative uses in many different areas where dynamic control over optical elements is wanted. Examples are endoscopic imaging through a multimode optical fiber [6], second harmonic imaging as e.g. used in stimulated emission depletion microscopy (STED) [7], focusing inside thick semitransparent objects and tissue [8], optical quantum encryption [9], laser welding [10] and many more. All these breakthroughs were made possible by the existence or development of so-called spatial light modulators, devices that allow for a programmable change of the phase of optical waves when passing through or being reflected from the modulator. Different designs exist based on liquid crystals [11,12], piezo controlled mirror segments [13], electrostatic or magnetic influencing of coated flexible membranes [14], shape changing flexible refractive elements as in mamal eyes [15] and many more. Each technology has its own advantages and disadvantages in terms of insertion losses, speed, constraints to what phase functions are allowed, pixel count, power handling of intense light beams, precision and so-on. In TEM, on the other hand, adaptive optical elements are commonplace. Indeed, even the simplest round magnetic or electrostatic lens, is tunable by either changing the current through the coils or by changing the potential difference over electrodes [16,17]. Adaptive optics is readily available on modern aberration corrected (S)TEM instruments in the form of complicated assemblies of multipolar lenses. They can be adaptively optimised on test samples to obtain the vastly improved resolution and current density that has formed the basis of most of the successes in experimental electron microscopy over the last decade [18–24]. Yet, aberration correctors in their current state don't allow for full flexibility in the phase they imprint on the electron wave. This is very apparent from the many attempts that have been, and are being made, towards a so-called Zernike phase plate for optimising the contrast in (weak) phase objects [25]. Indeed, if an aberration corrector would be able to change the phase on the optical axis by a given amount while leaving the rest of the wave unaffected there would be no need for the veritable zoo of different phase plate designs that exist. The magnetic vector potential in a magnetic multipole corrector is determined by the individual poles that act as boundary conditions to the free space in which the electrons travel. The vector potential component in the direction of electron motion obeys a Poisson equation:

$$\nabla^2 A_z - \frac{1}{c^2}\frac{\partial^2 A_z}{\partial^2 t} = -\mu_0 J_z, \tag{1}$$

assuming straight trajectories along z-direction through a thin region of space where the vector potential is non-zero. J_z represents the current density responsible for the creation of the local magnetic field, which can either come from the current carrying wires in e.g. a multipole lens, but also describes the magnetisation of any ferromagnetic cores by representing a virtual current flowing over the surface of these elements. The electron, due to the

Aharanov-Bohm effect, gets phase shifted by the projected magnetic vector potential A_z along its path as $\phi(x,y) = \frac{q}{\hbar}\int_{-\infty}^{\infty} A_z dz$. Assuming time independent solutions in free space ($J_z = 0$), we note that the obtainable phase plates are limited to a (small) subset of all possible phase plates constrained by a Laplace equation in 2D:

$$\nabla^2_{x,y}\phi = -\frac{q}{\hbar}\frac{\partial A_z}{\partial z}\Big|_{-\infty}^{\infty} = 0. \tag{2}$$

For thicker lenses (all realistic cases), the trajectory can deviate from the z-direction and more complicated arguments are needed, but in practice, for reasonable boundary conditions or multipole orders, the available phase plates generated by aberration correctors tend to be smooth. Fortunately, the available phase maps advantageously to the Zernike polynomials which are closely linked to the typical low order aberrations that are dominant in the electron microscope. However, a sharp change in phase in the center of the field as required for e.g. a Zernike phase plate would require prohibitively large magnetic multipole orders and is impractical for the foreseeable future.

To overcome this limitation, the assumption of free space has to be dropped (or alternatively dynamic fields are needed) and all current Zernike phase plates indeed consist of some form of material that is in contact with the electron wave. Some of the more promising designs create a miniaturised electrostatic einzel as originally proposed by Boersch in 1947 [26]. The advantage of this approach is that a tuneable local phase shift can be proposed. First experimental realisations date back to 1970 for an approximation by a charged wire [27] and later by a double loop design [28]. Actual einzel lens realisations were made after a design by Matsumoto et al [29] either by FIB [30] and by lithographic means allowing mass production and reproduceability [31–33]. Variants of these include a 3 fold axial variant and the so-called Zach phase plate, both making use of coaxial arrangements of an inner electrode with outside shielding [34–36]. The gain in flexibility offered by these electrostatic phase plates comes at the expense of admitting the material lens in the beam path resulting in a partial loss of electrons, decoherence, inelastic losses and charging issues [36,34,37]. A commercially available alternative, the Volta phase plate, uses local charge buildup on an insulating electron transparent film; but also here the free space requirement is dropped resulting in possible artefacts like drift, (in)elastic scattering, decoherence, uncontrolled charge and discharge [38–41]. So far, most phase plates have focused on phase contrast improvement and typically consist of a single region in space that is shifted in phase with respect to the rest of the wave that is left mostly unaltered. Increased flexibility in phase manipulation of electron waves recently gained considerable attention, showing exotic phase profiles as in electron vortices [42–47], Airy waves [48–50], helicon beams [51] or even the creation of an institute logo by modulating the phase profile of the wave [52]. Nearly all of these experiments make use of either holographic reconstruction using specif-

ically crafted phase [53–55,43] and or amplitude gratings [45,56] or refractive elements crafted with specific height profiles [44,53,57–60]. Even though these methods provide unprecedented flexibility in phase programming, offering a rich resource for the exploration of e.g. non-diffractive optical modes [61,62] , they suffer all from being static techniques. As such, a considerable time is required to create such phase plates and swap them in the aperture position of existing TEM microscopes which needs to be repeated with any new phase plate that is needed. Even when a wide selection of such phase plates is placed on a multi-aperture grid, new designs will come up and still necessitate replacements and the iterative optimisation is typically not possible.

In this paper we expand on these ideas by creating a rudimentary proof of concept of a programmable phase plate consisting of an array of 2x2 cylindrical electrodes, offering full dynamic control over the 4 individual phase plate elements. Even though the design has clear drawbacks in terms of total transmissivity, and limited pixel count, it nevertheless constitutes an important step towards a more generic programmable phase plate for TEM. In the remainder, we will give details on the design and fabrication of this phase plate followed by the first experimental results proving that a programmable multi-element phase plate for electrons is feasible. We continue by discussing the uses of such a limited phase plate and speculate about how much upscaling would be required to enable novel and exciting methods in the TEM [50]. It has to be noted here, that several alternative physical principles exist that allow control over the phase of electrons, most notably but not limited to e.g. electrostatic mirrors [63], magnetic vortex states [64,65], dynamic ponderomotive phase through the Kapitza Dirac effect [66,67]. These concepts can be exploited to create similar or even better devices, but we focus here on the description of what we believe to be the first truly versatile programmable phase array for electrons.

2 Experiment

In order to prepare an array of electrostatic phase shifting elements as sketched in fig. 1.a, a set of cylindrical electrodes needs to be created, sandwiched ideally between two ground planes. Here we simplified the setup considerably by working with a single large ground plane on which four independent cylinder electrodes are placed. The omission of the top ground plane will lead to a minor leaking of the potential of one cylinder into the space above a neighbouring cylinder electrode. This effect results in a small amount of crosstalk between the electrodes which can be partially compensated by altering the individual potentials to obtain the desired phase profile. The setup resembles an array of einzel lenses with the omission of the top ground plane but we will avoid the name einzel lens throughout the remainder of the manuscript to make this

distinction and because the lensing function of these lenses is deliberately kept so low that the dominant effect is a pure phase shift depending on the total projected potential. This also means that at the low voltages that are being used, possible aberrations caused by the lenses are negligible compared to the phase shifting effect .

A numerical solution of the Poisson equation with Dirichlet boundary conditions for the setup is presented in fig.2 making use of a home-built Liebmann algorithm in Matlab using a 3D cartesian grid of 500^3 voxels and shows the four electrodes at different potential in fig.2a. The voxel size was $(24.05\ nm)^3$ in the final simulation so that the simulated volume was $(12\ \mu m)^3$. The calculation was stopped when the maximum potential change between subsequent cycles went below 0.015mV. A cross section through 2 neighbouring electrodes in fig2b shows the fringing fields above the electrodes which lead to some cross talk.

The projected potential is shown in fig.2c expressed in units of phase assuming 300 kV electrons and with a target phase of $0, 1/2\pi, \pi, 3/2\pi$ for each electrode respectively. The relative deviation from the intended flat phase in each electrode is plotted in fig.2d showing the cross talk effect leading to phase errors of less than 0.07π in this case. Future geometrical optimisation could reduce this effect further or alternatively a top ground electrode would make this effect negligible at the expense of a more complicated setup.

It is worthwhile noting that for a single true axially symmetric einzel lens, having a top and bottom ground electrode Matsumoto et al. have proven that a flat phase profile is obtained, regardless of the dimensions of the lens as long as the lens is weakly excited [29]. Later, Glaeser et al. extended this statement to arbitrary shaped holes, allowing for non-axial symmetric boundary conditions that have a varying potential on the boundary and showed that in this case the phase plate can at most vary in a quadratic way over the aperture [68].

The device fabrication starts from a commercial Si_3N_4 TEM sample grid with a 200 nm $250\times250\ \mu m^2$ square membrane. The grid was coated on both sides with about 500 nm of gold, making use of a Balzers SCD 004 sputter coater. Masks were used to make sure the top and bottom layer are not electrically contacted. In the next step, four platinum cylinders of 1.4 μm height were deposited on the top gold surface by focused ion beam induced deposition (FIBID) using an FEI Helios Nanolab. The cylinders are placed on a square grid with a distance of approximately 2.5 μm from center to center. The four cylinders were then electrically insulated from each other by FIB milling the top layer of gold until reaching the underlying SiN membrane. Thanks to the large atomic number difference between the gold and the SiN membrane,it was possible to mill proper electrodes without milling through the SiN membrane, ensuring good insulation between the bottom ground electrode and the four

top electrodes. As a final step, 1 μm circular holes were drilled in the Pt cylinders all the way through the stacked layers to let the electron beam pass. The 1 μm diameter was chosen in order to have an aspect ratio between diameter and height of the cylindrical electrodes of approximately 1. This provides a rather homogeneous potential profile inside the tubular electrode as can be judged from the electrostatic simulation in fig.2.

The device was placed in a Dens Solutions Wildfire in-situ heating chip holder on top of a sacrificial heating chip, only used for contacting (heater window mechanically removed). The final contacts from the heating chip to the SiN grid are made with silver paint. Then, conductivity between the electrodes or between the electrodes and ground were carefully checked with a Keithley 2400 Source Meter and possible short circuits are corrected by further ion milling if necessary. The device was finally placed under vacuum conditions to allow for outgassing prior to insertion in the transmission electron microscope.

Once the contact holder was inserted in an aberration corrected FEI Titan^3 microscope (operating at 300 kV), the assembly was connected to a Keithley 2400 Source Meter to provide a programmable voltage source to specific electrodes while grounding the others. In the case of the vortex state (see below), a 100 Ohm resistor divider network provides a series of linearly increasing voltages to the subsequent electrodes. The ground of the voltage source was connected to the microscope ground while the body of the contact holder remains at a small potential to allow for pole touch sensing. There is not electrical contact between the body of the holder and the chip carrier. The microscope was operated in Lorentz mode with a strongly defocused monochromator in order to obtain sufficient spatial coherence in the sample plane to cover the four phase shifting elements. The apertures were then illuminated with a very good approximation of an electron plane wave. By going in diffraction mode, it was possible to observe the far field pattern of the four apertures. The diffraction pattern was recorded both in focus and defocused by 500 nm to better visualize the interference formed by the four individual electron wave patches that travel through the four aperture holes.

When all electrodes are grounded, the pattern displayed in fig.3 is obtained. One can observe a clear constructive interference between the four patches in the defocused case. Another pattern was obtained by applying a voltage to the two right electrodes until destructive interference between the left/right patch occurs. This requires approximately 300 mV with some deviation over the different electrodes due to remaining leakage current issues between the electrodes and the height of each cylinder not being exactly the same. This demonstrates that indeed the pixel elements influence the phase of the electron wave by π. It is then possible to estimate the sensitivity of the phase to the potential with a back-of the-envelope calculation making use of the interaction constant of $\sigma = 6.5\ V^{-1}\mu m^{-1}$ for 300 kV electrons and a tube length of

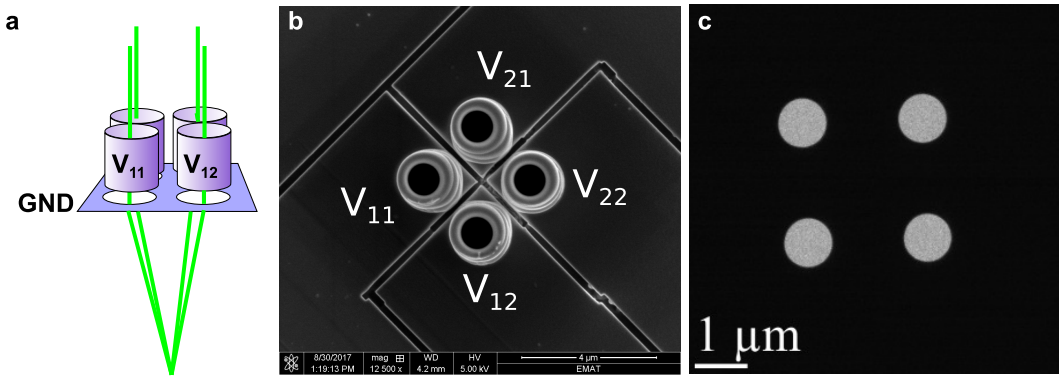

Fig. 1. (a) sketch of an array of cylindrical electrodes individually controlling the phase of 4 electron beams which recombine in the far field to form a programmable interference pattern. (b) SEM image of a proof of concept implementation of a 2x2 phase plate prepared as described in this paper. (c) TEM image of the aperture showing the geometry of the 4 aperture holes as well as the limited fill factor.

1.4 μm. For a π phase shift, this would require 350 mV which is in approximate agreement with the experimental values. A more accurate estimate can be made with the potential simulation presented in fig.2 and leads to an estimated 205 mV needed to obtain pi phase shift, more accurately taking into acount potential inhomogeneities and fringe fields. The result however depends in an sensitive manner on the exact geometry which only approximately matches the actual shape of the device.

In a similar manner, a voltage difference between up and down electrodes can be applied. As expected, the interference pattern has now up down symmetry with a destructive interference between the up down patches. A quadrupolar pattern and vortex pattern can also be generated, proving that a functional 2x2 programmable phase plate has been created. The obtained interference patterns very closely match the simulated patterns given in fig.4, assuming a true flat programmable phase plate device.

The high contrast of the interference patterns in fig.3 shows that decoherence effects are not detrimental in the current setup. An intensity profile across the central series of fringes of the situation with all electrodes grounded is given in fig.5a. The line profile is compared with a similar line scan over the simulated image as in the top-left of fig.4 but now including the measured point spread function of our CCD camera. We estimate the experimental fringe contrast to be approximately 55 % while the simulation predict a contrast of 64 % assuming the incoming electron beam to be fully coherent. This shows that decoherence effects caused by interaction with the electrodes is minor especially as it is unlikely that the incoming electron beam was in a fully coherent state. Alternatively we investigate the occurrence of inelastic losses which could cause unwanted spectroscopic signals and decoherence. We performed low loss electron energy loss spectroscopy using a focused STEM probe (convergence angle

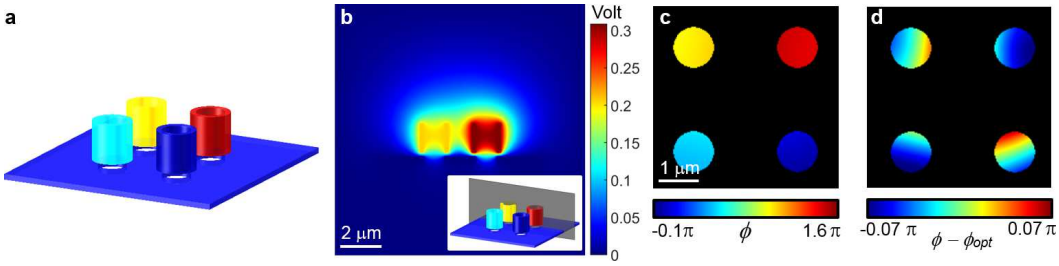

Fig. 2. Simulated potential of the setup (a) showing the four electrodes at different potential of $0, 103, 206, 309$ mV in order to obtain $0, 1/2\pi, \pi, 3/2\pi$ phase shift. A slice through 2 neighbouring electrodes (b) shows the potential homogeneity inside the cylinders with fringe fields extending above the electrodes due to the missing top ground plane. The projected potential is shown in (c) in units of phase shift assuming 300 kV electrons. The difference with the intended phase plate of $0, 1/2\pi, \pi, 3/2\pi$ is shown in (d) with a maximum deviation that remains below 0.07π as a result from the cross talk between the neighbouring pixels due to the lack of a top ground plane.

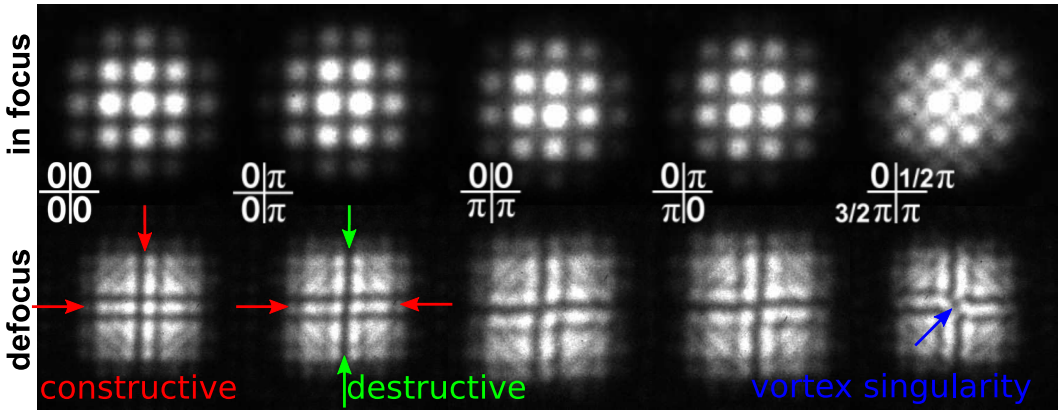

Fig. 3. (top row) Set of diffraction pattern for 5 different applied potential configurations leading to an approximate realisation of the phase symmetry as indicated on each panel. (bottom row) Defocused diffraction patterns for the same potential configuration showing more directly the constructive and destructive interference features between the 4 patches as indicated by arrows.

$\alpha = 20$ mrad, 300kV, collection angle $\beta = 11$ mrad) passing through a single phase shifting element. Fig.5b shows the low loss spectrum when a focused electron probe is positioned in the center of the element as compared to the spectrum averaged over a 2D scanned area covering the full phase shift element area. This shows that less than 2.4 % of the electrons suffer a low loss event in the plasmon range up to 45 eV. This is not surprising as only those electrons that pass very close to the inner walls of the cylinder electrodes are in the ability to excite such inelastic events, with a typical delocalisation in the nanometer range. As this delocalisation distance is very small compared to the diameter of the hole, the probability for inelastic scattering is negligible at the current dimensions. Both fringe contrast and EELS observations show that at the current dimensions and materials used, the programmable phase

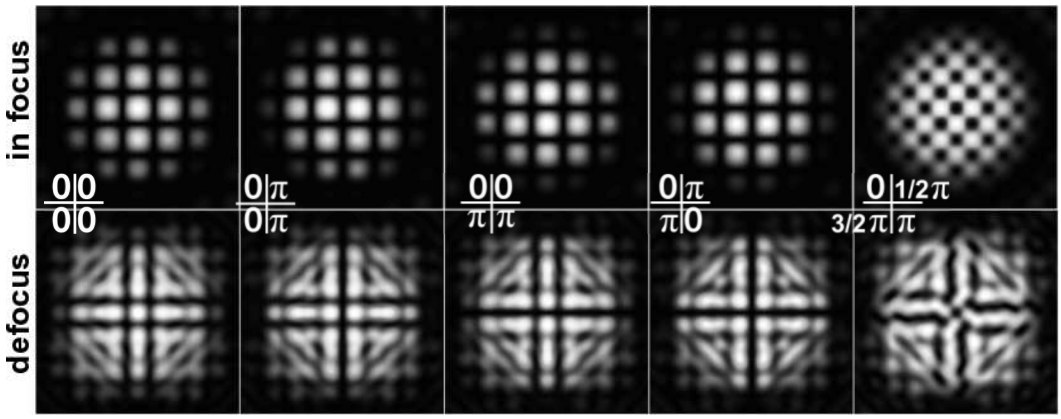

Fig. 4. Simulated diffraction patterns assuming an ideal programmable phase shifting device with dimensions matching the experiment. Note the strong similarity in the intensity patterns for both in focus (top row) and defocused diffraction pattern series.

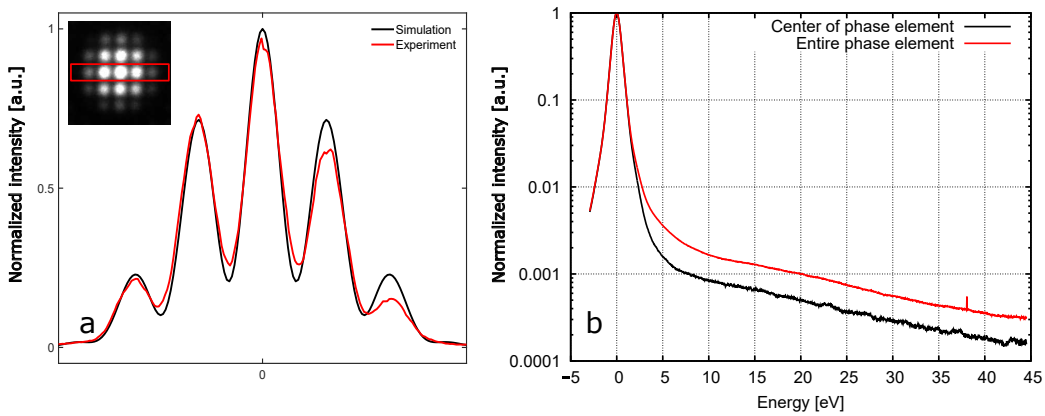

Fig. 5. a) Fringe contrast integrated from a central region of the experiment with all electrodes grounded (red) as shown in inset compared to a similar region from the simulated profile (black) taking into account the experimental point spread function of the detector. Fringe contrast is estimated as 55% while the simulation shows an expected contrast of 64% assuming a fully coherent incoming electron beam. This shows the excellent preservation of coherence through the device. b) Low loss EELS spectra obtained after passing a focused STEM probe through the center of a phase shift element (black) and integrated over the whole area of the element (red). Less than 2.4% of the electrons passing through the phase shifting element undergo inelastic scattering and could suffer unwanted loss of coherence. Both a) and b) show that at the current dimensions and choice of materials, decoherence and inelastic effects are minor.

plate performs excellent in terms of decoherence and inelastic losses.

3 Discussion

The above experimental results demonstrate the feasibility of a multi-element programmable phase plate for use in electron microscopy. This holds clear promise for future work but several shortcomings of the current implementation will need to be addressed. The most important shortcoming lies in the inherent material making up the pixel element electrodes, blocking part of the electron beam. In the current demonstration this allows only about 12% of the incoming beam to pass through the 4 individual phase shifters. Undoubtedly this so-called fill-factor can be increased substantially in later designs, but it is hard to imagine a design which would allow passing substantially more than 50%. The fill-factor will of-course depend heavily on the micro machining or lithographic capabilities that will be used in further iterations of the design. As long as the phase plate is used in setups that shape the electron beam before the sample, this does not have to be a significant drawback, as modern instruments often provide more current or electron dose than the sample can handle, and losing a fraction of this current would not limit the usability of the device. Changing the phase behind the sample, as typical in e.g. setups for Zernike weak phase imaging, would suffer significantly from a less than unity transmitivity and it seems rather unfavourable to block electrons that carry precious information on beam sensitive materials. If however, this loss of electrons is compensated by a greater gain in contrast, it could still turn out beneficial. The blocking nature of the phase shifting structure shares however the significant drawback with other electrostatic Zernike phase plate designs that it throws away important low frequency information when used in the back focal plane, after the sample [69,35]. In order to upscale the device to a higher pixel count, lithographic techniques will be required and interconnect density may quickly put a limit to the maximum attainable number of pixels that each need to be individually contacted to a programmable voltage source. Matrix adressing methods such as those used in dynamic random acces memories could solve this, but require a nonlinear switching element, such as e.g. a transistor, integrated in the vicinity of each pixel element. Implementing such schemes should allow for pixel arrays of thousands to millions of pixel elements. One could wonder how many elements would be needed to provide ultimate flexibility in phase shaping the electron beam. As a demonstration, we compare the usefulness of a modest 55 and more elaborate 2205 pixel phase plate to act as a probe-C_s corrector device in fig 6. We assumed a spherical aberration coefficient of $C_s = 1$ mm at 300 keV and compare to an uncorrected system at Scherzer defocus and to a fully corrected system, fixing the opening (half) angle at 20 mrad. From the simulation we see that the 55 pixel variant shows some benefit in terms of reduced tails on the probe intensity (b,f) which results in a sharper intensity radial profile in fig.6.i as compared to the uncorrected situation. Increasing the pixel count to 2205 results in a much sharper probe with a very simmilar profile (c,g) as the diffraction lim-

ited profile of the fully corrected situation (d,h). This demonstrates that such phase plates could eventually start replacing magnetic multipole aberration correctors in the probe-forming system of TEM microscopes, but clearly a substantial amount of pixels would be needed. A full exploration of the ideal position, shape and number of pixels for aberration correction with a programmable phase plate will provide a rich arrea of further research, but is beyond the scope of the current discussion. Nevertheless, aberration correction was not the first goal of the current implementation and low pixel element devices like the one presented here, or slightly upscaled can serve as a very useful experimenting platform for beam shaping and exploring other applications that focus more on tuning the phase of the electron wave to bring out specific contrast. Examples include the study of non-diffracting electron beams[61,54,70–73,48], symmetry mapping of plasmonic excitations[74], mapping of magnetic fields [45,75–79] or edge contrast enhancement [76]. In optics, very useful spatial light modulators exist consisting of only 37 elements [80], even though they often provide a linear phase ramp in each pixel element which can also be imagined for electrons with a slight complication of the design where each cylindrical electrode is split in 3 separate planar electrodes providing a linear potential profile in triangular or hexagonal pixel elements. The optimised pattern of pixel elements depends on the intended use, but in low pixel count designs, it is likely that some form of radial pattern will be the most efficient. In order to demonstrate some of the capabilities that e.g. a radially oriented 55 pixel phase plate would bring, we show in fig. 7 the capability of such a simple phase plate to create approximations to some well-known Hermite Gaussian and Laguerre Gaussian modes that are abundant in optics research. This capability would open up the field of beam shaping TEM providing a very desirable flexibility in the quantum state of the electron probe, much like what current spatial light modulators offer in optics. The fact that such a phase plate could rapidly switch between such modes could allow for differential measurements bringing out the specific contrast that comes with a certain probe symmetry and directly compare it to a near-simultaneous experiment done with another probe symmetry. As such, this development could bring the field of beam shaping to a significantly higher level.

Given the above demonstration that an upscaled version of the presented 2x2 device could have multiple uses, we can look into possible obstacles that could hinder progress. Indeed, the presence of the pixel electrodes can have unwanted effects, such as charging or decoherence due to thermal current flowing in the electrode material [81–83]. The current implementation did not show either of these effects to be significant as can be seen by the high fringe contrast in fig.**??**. Increasing the pixel density could eventually make these effects more prominent. In this respect, the short length (1.4 μm) over which the electrons interact with the pixel electrodes, helps to limit the decoherence effect substantially as they are expected to scale with interaction length and inversely with the square of tube radius [82]. Cooling could further help to keep decoherence

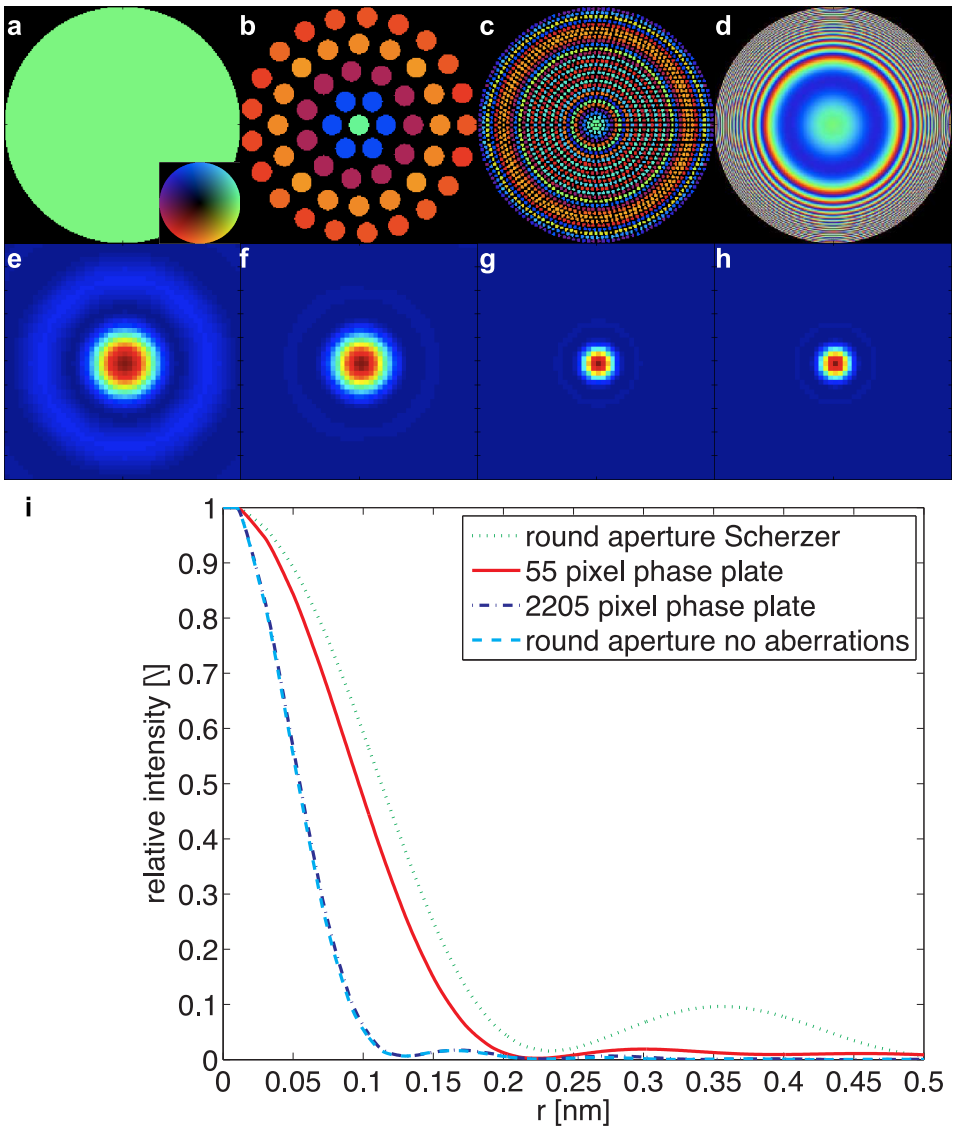

Fig. 6. Simulated performance of a programmable phase plate as a C_s corrector assuming 300 keV and C_s=1 mm. Two phase plates are simulated, a modest 55 pixel plate and a more demanding 2205 pixel phase plate. The defocus of the lens system was optimised to -75 nm and -250 nm respectively to reach the optimum probe shape. The result is compared to an ideal aberration free system with the same round aperture with opening angle 20 mrad. The resulting probe intensities are shown respectively in (e,f,g,h), the images have dimension 1x1 nm. The azimuthally averaged probe intensity is shown in (i). Note that the low pixel count phase plate in (b) does not significantly improve the probe size but does improve the tails. Introducing significantly more pixels (c) approaches the ideal case quite closely. Note that even though the probe appears similar to the ideal diffraction limited case (d), a significant amount of the probe intensity is scattered to higher angles due to the narrow pixel shape function which would lead to an increased background when using this probe for imaging. The colorwheel shown as inset in (a) shows the colorscale used in (a,b,c,d) to depict both amplitude as intensity and phase as hue.

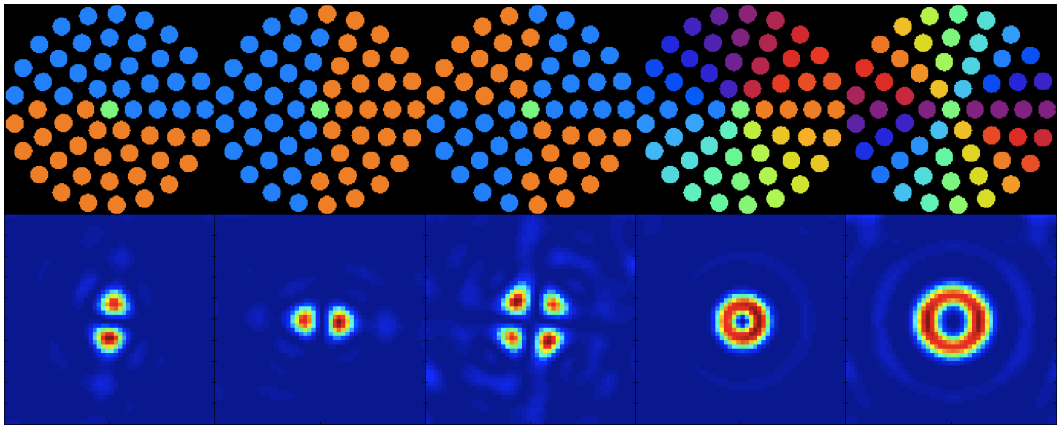

Fig. 7. A series of exotic electron beams prepared with a modest programmable phase plate (55 pixels, 41% fill-factor) approximating (from left to right) $HG_{0,1}$, $HG_{1,0}$, $HG_{1,1}$, $LG_{0,1}$, $LG_{0,2}$. This shows that even a modest programmable phase plate can be very useful for producing exotic beam types that where hithertho difficult to produce in a TEM requiring time consuming and static (holographic) phase plates.

low, but is rather unattractive from a practical point of view. Contamination, could be another limitation of the design as small amounts of contamination could block pixels and render the whole array useless. We did not observe such contamination or related charging effects during the current experiments even though we did not perform extended irradiation experiments. Nevertheless, the situation of a phase plate for probe forming as suggested here is far more relaxed when compared to the high localised intensities that occur in a typical Boersch phase plate setup in the objective plane, where contamination is an important concern [34]. If, however, contamination would turn out to be an issue in future designs, a heating element could alleviate the problem.

Spatial coherence length limitations in the aperture plane are not much more demanding as for current aberration corrected STEM instruments where typically apertures up to 50 μm can be illuminated with sufficient coherence. This puts constraints on the diameter of the individual phase shifting elements and would require elements of the order of 100 nm diameter to obtain high pixel count phase plates as simulated in fig.6c. Such small diameters will likely introduce more decoherence and inelastic scattering as compared to more modest pixel counts. If this would turn out to be a serious issue, there is still the option to include an extra set of magnification and demagnification lenses to increase the size of the coherently illuminated patch and to scale the dimensions of the device accordingly as has been succesfully applied to Boersch phase plate setups [34].

An important advantage of the presented device is the relative insensitivity of the performance to the quality of the voltage sources driving the pixel electrodes. Indeed in the current dimensions, a voltage of the order of a few 100 mV

suffices to create a 2π phase shift. As phase is defined modulo 2π and because neighbouring patches of electron waves are divided by opaque walls of the pixel elements, there is no need to apply for more phase shift than this, similar to an optical Fresnel lens. This leads to a very relaxed requirement on the quality and noise performance of the voltage source. Indeed, even an idealised 8 bit digital to analog converter could provide a more than sufficient $2\pi/256$ phase resolution. This relative insensitivity of the phase to the potential also allows for very fast settling times in combination with a very low capacitance of the pixel elements with respect to each other and to the ground plane. As long as all pixels are driven from individual voltage sources (DA converters), a response speed in the range of micro to nanoseconds seems entirely feasible. Upscaling to more than e.g. 10x10 pixels will likely require matrix addressing as is commonly used in microelectronics for e.g lcd screens and DRAM memory. This would require at least one active element per pixel in the form of e.g. a multi-gate field effect transistor allowing the addressing of an individual pixel through the simultaneous firing of row and column signal charging the individual pixel to a desired potential. At current densities of DRAM, such matrix scheme could be realised without requiring substantial extra area as long as the transistors can be protected adequately against radiation damage. However, matrix addressing might limit the programming speed considerably depending on the design. Such rapidly changing phase plates could allow for autotuning and iterative measurement schemes which profit from the total absence of hysteresis effects that hamper all ferromagnetic core based optical elements in conventional TEM instruments.

4 Conclusion

We have demonstrated a proof of concept device that allows to dynamically control the phase of 2x2 segments of a coherent electron beam in a transmission electron microscope. The experimental implementation and first results demonstrate that such a device holds promise for upscaling towards a more useful higher number of pixels. Several design considerations and directions for further research are discussed. These make plausible that the presented proof of concept marks just the beginning of an exciting development that could alter the way how one thinks about electron optics, providing vastly increased flexibility, speed, repeatability and offering novel iterative measurement protocols that are difficult if not impossible to implement with current electron optical technology.

5 acknowledgments

J.V. and A.B. acknowledge funding from the Fund for Scientific Research Flanders FWO project G093417N and the European Research Council under the 7th Framework Program (FP7), ERC Starting Grant 278510 VORTEX and ERC proof of concept project DLV-789598 ADAPTEM. The Qu-Ant-EM microscope used in this work was partly funded by the Hercules fund from the Flemish Government. MdH acknowledges financial support from the ANR-COSMOS (ANR-12-JS10-0002). MdH and ML acknowledge funding from the Laboratoire d'excellence LANEF in Grenoble (ANR-10-LABX-51-01).

References

[1] D L Fried. Optical Resolution Through a Randomly Inhomogeneous Medium for Very Long and Very Short Exposures. *Journal of the Optical Society of America*, 56(10):1372, oct 1966.

[2] Richard Davies and Markus Kasper. Adaptive Optics for Astronomy. *Annual Review of Astronomy and Astrophysics*, 50(1):305–351, sep 2012.

[3] J Y Wang. Optical Resolution through a Turbulent Medium with Adaptive Phase Compensations*. *Journal of the Optical Society of America*, 67(3):383, mar 1977.

[4] F Merkle, P Kern, P Lena, F Rigaut, J C Fontanella, G Rousset, C Boyer, J P Gaffard, and P Sagourel. Successful Tests of Adaptive Optics. *The Messenger*, 58:1–4, 1989.

[5] Daniel Clery. Building James Webb: The Biggest, Boldest, Riskiest Space Telescope. *Science*, feb 2016.

[6] Reza Nasiri Mahalati, Ruo Yu Gu, and Joseph M Kahn. Resolution Limits for Imaging through Multi-Mode Fiber. *Optics Express*, 21(2):1656, jan 2013.

[7] Stefan W Hell and Jan Wichmann. Breaking the Diffraction Resolution Limit by Stimulated Emission: Stimulated-Emission-Depletion Fluorescence Microscopy. *Optics Letters*, 19(11):780, jun 1994.

[8] Martin J Booth. Adaptive Optical Microscopy: The Ongoing Quest for a Perfect Image. *Light: Science and Applications*, 3(4):e165, apr 2014.

[9] Pere Clemente, Vicente Durán, Víctor Torres-Company, Enrique Tajahuerce, and Jesús Lancis. Optical encryption based on computational ghost imaging. *Optics letters*, 35(14):2391–3, jul 2010.

[10] Libor Mrna, Martin Šarbort, Šimon Rerucha, and Peter Jedlička. Adaptive optics for control of the laser welding process. *EPJ Web of Conferences 48*, 17:1–7, 2013.

[11] C Slinger, C Cameron, and M Stanley. Computer-Generated Holography as a Generic Display Technology. *Computer*, 38(8):46–53, aug 2005.

[12] Yasunori Igasaki, Fanghong Li, Narihiro Yoshida, Haruyoshi Toyoda, Takashi Inoue, Naohisa Mukohzaka, Yuji Kobayashi, and Tsutomu Hara. High Efficiency Electrically-Addressable Phase-Only Spatial Light Modulator. *Optical Review*, 6(4):339–344, 1999.

[13] Ehud Steinhaus and S G Lipson. Bimorph piezoelectric flexible mirror. *Journal of the Optical Society of America*, 69(3):478–481, 1979.

[14] Gleb Vdovin and P. M. Sarro. Flexible mirror micromachined in silicon. *Applied Optics*, 34(16):2968, jun 1995.

[15] Kuang-Sheng Hong, Jing Wang, Alexey Sharonov, Dinesh Chandra, Joanna Aizenberg, and Shu Yang. Tunable microfluidic optical devices with an integrated microlens array. *Journal of Micromechanics and Microengineering*, 16(8):1660–1666, 2006.

[16] Harald Rose. *Geometrical Charged-Particle Optics*, volume 142 of *Springer Series in Optical Sciences*. Springer Berlin Heidelberg, Berlin, Heidelberg, 2009.

[17] P.W. Hawkes and E. Kasper. *Front Matter*. Elsevier, 1994.

[18] M Haider, P Hartel, H Muller, S Uhlemann, and J Zach. Current and Future Aberration Correctors for the Improvement of Resolution in Electron Microscopy. *Philosophical Transactions of the Royal Society A: Mathematical, Physical and Engineering Sciences*, 367(1903):3665–3682, sep 2009.

[19] R M Tromp, J B Hannon, A W Ellis, W Wan, A Berghaus, and O Schaff. A New Aberration-Corrected, Energy-Filtered LEEM/PEEM Instrument. I. Principles and Design. *Ultramicroscopy*, 110(7):852–861, jun 2010.

[20] P E Batson, N Dellby, and O L Krivanek. Sub-Ångstrom Resolution Using Aberration Corrected Electron Optics. *Nature*, 418(6898):617–620, aug 2002.

[21] H Rose. Prospects for Aberration-Free Electron Microscopy. *Ultramicroscopy*, 103(1):1–6, apr 2005.

[22] H Rose. Phase-Contrast in Scanning-Transmission Electron-Microscopy. *Optik*, 39(4):416–436, 1974.

[23] Martin Linck, Peter Hartel, Stephan Uhlemann, Frank Kahl, Heiko Müller, Joachim Zach, Max. Haider, Marcel Niestadt, Maarten Bischoff, Johannes Biskupek, Zhongbo Lee, Tibor Lehnert, Felix Börrnert, Harald Rose, and Ute Kaiser. Chromatic Aberration Correction for Atomic Resolution TEM Imaging from 20 to 80 kV. *Physical Review Letters*, 117(7), aug 2016.

[24] M Haider, S Uhlemann, E Schwan, H Rose, B Kabius, and K Urban. Electron Microscopy Image Enhanced. *Nature*, 392(6678):768–769, 1998.

[25] F Zernike. Phase Contrast, a New Method for the Microscopic Observation of Transparent Objects. *Physica*, 9(7):686–698, jul 1942.

[26] Hans Boersch. Über die Kontraste von Atomen im Elektronenmikroskop. *Zeitschrift fur Naturforschung - Section A Journal of Physical Sciences*, 2(11-12):615–633, 1947.

[27] P. N. T. Unwin. An Electrostatic Phase Plate for the Electron Microscope. *Berichte der Bunsengesellschaft für physikalische Chemie*, 74:1137–1141, 1970.

[28] Rossana Cambie, Kenneth H. Downing, Dieter Typke, Robert M. Glaeser, and Jian Jin. Design of a microfabricated, two-electrode phase-contrast element suitable for electron microscopy. *Ultramicroscopy*, 107(4-5):329–339, 2007.

[29] Takao Matsumoto and Akira Tonomura. The phase constancy of electron waves traveling through Boersch's electrostatic phase plate. *Ultramicroscopy*, 63(1):5–10, apr 1996.

[30] Andreas Walter, Heiko Muzik, Henning Vieker, Andrey Turchanin, André Beyer, Armin Gölzhäuser, Manfred Lacher, Siegfried Steltenkamp, Sam Schmitz, Peter Holik, Werner Kühlbrandt, and Daniel Rhinow. Practical aspects of Boersch phase contrast electron microscopy of biological specimens. *Ultramicroscopy*, 116:62–72, 2012.

[31] Sen Hui Huang, Wan Jhih Wang, Chia Seng Chang, Yeu Kuang Hwu, Fan Gang Tseng, Ji Jung Kai, and Fu Rong Chen. The fabrication and application of Zernike electrostatic phase plate. *Journal of Electron Microscopy*, 55(6):273–280, 2006.

[32] D. Alloyeau, W. K. Hsieh, E. H. Anderson, L. Hilken, G. Benner, X. Meng, F. R. Chen, and C. Kisielowski. Imaging of soft and hard materials using a Boersch phase plate in a transmission electron microscope. *Ultramicroscopy*, 110(5):563–570, 2010.

[33] B. Barton, D. Rhinow, A. Walter, R. Schröder, G. Benner, E. Majorovits, M. Matijevic, H. Niebel, H. Müller, M. Haider, M. Lacher, S. Schmitz, P. Holik, and W. Kühlbrandt. In-focus electron microscopy of frozen-hydrated biological samples with a Boersch phase plate. *Ultramicroscopy*, 111(12):1696–1705, 2011.

[34] Andreas Walter, Siegfried Steltenkamp, Sam Schmitz, Peter Holik, Edvinas Pakanavicius, Roland Sachser, Michael Huth, Daniel Rhinow, and Werner Kühlbrandt. Towards an optimum design for electrostatic phase plates. *Ultramicroscopy*, 153:22–31, jun 2015.

[35] Katrin Schultheiss, Joachim Zach, Bjoern Gamm, Manuel Dries, Nicole Frindt, Rasmus R Schröder, and Dagmar Gerthsen. New Electrostatic Phase Plate for Phase-Contrast Transmission Electron Microscopy and Its Application for Wave-Function Reconstruction. *Microscopy and Microanalysis*, 16(06):785–794, dec 2010.

[36] Nicole Frindt, Marco Oster, Simon Hettler, Björn Gamm, Levin Dieterle, Wolfgang Kowalsky, Dagmar Gerthsen, and Rasmus R Schröder. In-Focus Electrostatic Zach Phase Plate Imaging for Transmission Electron Microscopy with Tunable Phase Contrast of Frozen Hydrated Biological Samples. *Microscopy and Microanalysis*, 20(01):175–183, feb 2014.

[37] S Hettler, M Dries, J Zeelen, M Oster, R R Schröder, and D Gerthsen. High-Resolution Transmission Electron Microscopy with an Electrostatic Zach Phase Plate. *New Journal of Physics*, 18(5):53005, may 2016.

[38] Radostin Danev and Wolfgang Baumeister. Cryo-EM Single Particle Analysis with the Volta Phase Plate. *Elife*, 5, mar 2016.

[39] Radostin Danev, Robert M Glaeser, and Kuniaki Nagayama. Practical Factors Affecting the Performance of a Thin-Film Phase Plate for Transmission Electron Microscopy. *Ultramicroscopy*, 109(4):312–325, mar 2009.

[40] Radostin Danev and Kuniaki Nagayama. Single Particle Analysis Based on Zernike Phase Contrast Transmission Electron Microscopy. *Journal of Structural Biology*, 161(2):211–218, feb 2008.

[41] R Danev, B Buijsse, M Khoshouei, J M Plitzko, and W Baumeister. Volta Potential Phase Plate for In-Focus Phase Contrast Transmission Electron Microscopy. *Proceedings of the National Academy of Sciences*, 111(44):15635–15640, nov 2014.

[42] K.Y. Bliokh, I.P. Ivanov, G. Guzzinati, L. Clark, R. Van Boxem, A. Béché, R. Juchtmans, M.A. Alonso, P. Schattschneider, F. Nori, and J. Verbeeck. Theory and applications of free-electron vortex states. *Physics Reports*, 690:1–70, may 2017.

[43] Benjamin J McMorran, Amit Agrawal, Ian M Anderson, Andrew a Herzing, Henri J Lezec, Jabez J McClelland, and John Unguris. Electron vortex beams with high quanta of orbital angular momentum. *Science (New York, N.Y.)*, 331(6014):192–195, 2011.

[44] Masaya Uchida and Akira Tonomura. Generation of electron beams carrying orbital angular momentum. *Nature*, 464(7289):737–9, apr 2010.

[45] J Verbeeck, H Tian, and P Schattschneider. Production and application of electron vortex beams. *Nature*, 467(7313):301–304, 2010.

[46] A. Béché, R. Juchtmans, and J. Verbeeck. Efficient creation of electron vortex beams for high resolution STEM imaging. *Ultramicroscopy*, pages 1–8, may 2016.

[47] Christopher J. Edgcombe. Phase Plates for Transmission Electron Microscopy. In *Advances in Imaging and Electron Physics*, chapter 2, pages 61–102. Elsevier, 2017.

[48] Noa Voloch-Bloch, Yossi Lereah, Yigal Lilach, Avraham Gover, and Ady Arie. Generation of Electron Airy Beams. *Nature*, 494(7437):331–335, feb 2013.

[49] Ido Kaminer, Jonathan Nemirovsky, Mikael Rechtsman, Rivka Bekenstein, and Mordechai Segev. Self-accelerating Dirac particles and prolonging the lifetime of relativistic fermions. *Nature Physics*, 11(January):261–267, 2015.

[50] Giulio Guzzinati, Laura Clark, Armand Béché, Roeland Juchtmans, Ruben Van Boxem, Michael Mazilu, and Jo Verbeeck. Prospects for versatile phase manipulation in the TEM: Beyond aberration correction. *Ultramicroscopy*, 151:85–93, apr 2015.

[51] Roy Shiloh and Ady Arie. 3D Shaping of Electron Beams Using Amplitude Masks. *Ultramicroscopy*, 177:30–35, jun 2017.

[52] Roy Shiloh, Yossi Lereah, Yigal Lilach, and Ady Arie. Sculpturing the Electron Wave Function Using Nanoscale Phase Masks. *Ultramicroscopy*, 144:26–31, sep 2014.

[53] Vincenzo Grillo, Gian Carlo Gazzadi, Ebrahim Karimi, Erfan Mafakheri, Robert W. Boyd, and Stefano Frabboni. Highly efficient electron vortex beams generated by nanofabricated phase holograms. *Applied Physics Letters*, 104(4):1–5, 2014.

[54] Vincenzo Grillo, Ebrahim Karimi, Gian Carlo Gazzadi, Stefano Frabboni, Mark R Dennis, and Robert W Boyd. Generation of Nondiffracting Electron Bessel Beams. *Physical Review X*, 4(1), jan 2014.

[55] Halina Rubinsztein-Dunlop, Andrew Forbes, M V Berry, M R Dennis, David L Andrews, Masud Mansuripur, Cornelia Denz, Christina Alpmann, Peter Banzer, Thomas Bauer, Ebrahim Karimi, Lorenzo Marrucci, Miles Padgett, Monika Ritsch-Marte, Natalia M Litchinitser, Nicholas P Bigelow, C Rosales-Guzmán, A Belmonte, J P Torres, Tyler W Neely, Mark Baker, Reuven Gordon, Alexander B Stilgoe, Jacquiline Romero, Andrew G White, Robert Fickler, Alan E Willner, Guodong Xie, Benjamin McMorran, and Andrew M Weiner. Roadmap on Structured Light. *Journal of Optics*, 19(1):13001, jan 2017.

[56] J. Verbeeck, P. Schattschneider, S. Lazar, M. Stoger-Pollach, S. Loffler, A. Steiger-Thirsfeld, and G. Van Tendeloo. Atomic scale electron vortices for nanoresearch. *Applied Physics Letters*, 99(20):203109, 2011.

[57] A. Béché, R Winkler, H Plank, F Hofer, and J Verbeeck. Focused electron beam induced deposition as a tool to create electron vortices. *Micron*, 80:34–38, jan 2016.

[58] Roy Shiloh, Roei Remez, and Ady Arie. Prospects for Electron Beam Aberration Correction Using Sculpted Phase Masks. *Ultramicroscopy*, 163:69–74, apr 2016.

[59] Roy Shiloh, Roei Remez, Peng-Han Lu, Lei Jin, Yossi Lereah, Amir H Tavabi, Rafal E Dunin-Borkowski, and Ady Arie. Spherical Aberration Correction in a Scanning Transmission Electron Microscope Using a Sculpted Foil. *arXiv:1705.05232 [physics]*, may 2017.

[60] Vincenzo Grillo, Amir H. Tavabi, Emrah Yucelen, Peng-Han Lu, Federico Venturi, Hugo Larocque, Lei Jin, Aleksei Savenko, Gian Carlo Gazzadi, Roberto Balboni, Stefano Frabboni, Peter Tiemeijer, Rafal E. Dunin-Borkowski, and Ebrahim Karimi. Towards a holographic approach to spherical aberration

correction in scanning transmission electron microscopy. *Optics Express*, 25(18):21851, sep 2017.

[61] M V Berry and N L Balazs. Nonspreading Wave Packets. *American Journal of Physics*, 47(3):264–267, mar 1979.

[62] J. Durnin, J. Miceli, and J. H. Eberly. Diffraction-free beams. *Physical Review Letters*, 58(15):1499–1501, 1987.

[63] D Preikszas and H Rose. Correction Properties of Electron Mirrors. *Journal of Electron Microscopy*, 46(1):1–9, jan 1997.

[64] M K Hari, M Beleggia, and R M D Brydson. Occurrence of the vortex state for magnetic phase plates. *Journal of Physics: Conference Series*, 241(1):12069, 2010.

[65] C. J. Edgcombe. A phase plate for transmission electron microscopy using the Aharonov-Bohm effect. *Journal of Physics: Conference Series*, 241, 2010.

[66] B. Barwick and H. Batelaan. Aharonov-Bohm phase shifts induced by laser pulses. *New Journal of Physics*, 10, 2008.

[67] H. Müller, Jian Jin, R. Danev, J. Spence, H. Padmore, and R. M. Glaeser. Design of an electron microscope phase plate using a focused continuous-wave laser. *New Journal of Physics*, 12, 2010.

[68] Robert M. Glaeser and Holger Müller. Generalization of the Matsumoto-Tonomura approximation for the phase shift within an open aperture. *Ultramicroscopy*, 138:1–3, 2014.

[69] K Schultheiß, F Pérez-Willard, B Barton, D Gerthsen, and R R Schröder. Fabrication of a Boersch Phase Plate for Phase Contrast Imaging in a Transmission Electron Microscope. *Review of Scientific Instruments*, 77(3):33701, mar 2006.

[70] M R Lapointe. Review of Non-Diffracting Bessel Beam Experiments. *Optics and Laser Technology*, 24(6):315–321, dec 1992.

[71] J E Morris, T Čižmár, H I C Dalgarno, R F Marchington, F J Gunn-Moore, and K Dholakia. Realization of Curved Bessel Beams: Propagation around Obstructions. *Journal of Optics*, 12(12):124002, dec 2010.

[72] D McGloin and K Dholakia. Bessel Beams: Diffraction in a New Light. *Contemporary Physics*, 46(1):15–28, jan 2005.

[73] G A Siviloglou, J Broky, A Dogariu, and D N Christodoulides. Observation of Accelerating Airy Beams. *Physical Review Letters*, 99(21), nov 2007.

[74] Giulio Guzzinati, Armand Béché, Hugo Lourenço-Martins, Jérôme Martin, Mathieu Kociak, and Jo Verbeeck. Probing the Symmetry of the Potential of Localized Surface Plasmon Resonances with Phase-Shaped Electron Beams. *Nature Communications*, 8:14999, apr 2017.

[75] L Clark, A. Béché, G Guzzinati, and J Verbeeck. Quantitative measurement of orbital angular momentum in electron microscopy. *Physical Review A*, 89(5):053818, may 2014.

[76] Roeland Juchtmans, Laura Clark, Axel Lubk, and Jo Verbeeck. Spiral phase plate contrast in optical and electron microscopy. *Physical Review A*, 94(2):023838, aug 2016.

[77] Vincenzo Grillo, Tyler R. Harvey, Federico Venturi, Jordan S. Pierce, Roberto Balboni, Frédéric Bouchard, Gian Carlo Gazzadi, Stefano Frabboni, Amir H. Tavabi, Zi-An Li, Rafal E. Dunin-Borkowski, Robert W. Boyd, Benjamin J. McMorran, and Ebrahim Karimi. Observation of nanoscale magnetic fields using twisted electron beams. *Nature Communications*, 8(1):689, dec 2017.

[78] T. Schachinger, S. Löffler, A. Steiger-Thirsfeld, M. Stöger-Pollach, S. Schneider, D. Pohl, B. Rellinghaus, and P. Schattschneider. EMCD with an electron vortex filter: Limitations and possibilities. *Ultramicroscopy*, 179:15–23, aug 2017.

[79] P. Schattschneider, S. Löffler, M. Stöger-Pollach, and J. Verbeeck. Is magnetic chiral dichroism feasible with electron vortices? *Ultramicroscopy*, 136(4):81–5, jan 2014.

[80] Silvestre Manzanera, Michael A. Helmbrecht, Carl J. Kempf, and Austin Roorda. MEMS segmented-based adaptive optics scanning laser ophthalmoscope. *Biomedical Optics Express*, 2(5):1204, may 2011.

[81] Stephan Uhlemann, Heiko Müller, Joachim Zach, and Max. Haider. Thermal magnetic field noise: Electron optics and decoherence. *Ultramicroscopy*, 151:199–210, apr 2015.

[82] Stephan Uhlemann, Heiko Müller, Peter Hartel, Joachim Zach, and Max. Haider. Thermal Magnetic Field Noise Limits Resolution in Transmission Electron Microscopy. *Physical Review Letters*, 111(4), jul 2013.

[83] Archie Howie. Addressing Coulomb's Singularity, Nanoparticle Recoil and Johnson's Noise. *Journal of Physics: Conference Series*, 522:12001, jun 2014.